Thermal properties of nanoporous gold

Anatoly I. Frenkel,[1,*] Relja Vasić,[1] Bluma Dukesz,[1] Diya Li,[2] Mingwei Chen,[3] Ling Zhang,[3] and Takeshi Fujita[3,4]
[1]*Department of Physics, Yeshiva University, 245 Lexington Avenue, New York, New York 10016, USA*
[2]*Department of Chemical and Biomolecular Engineering, University of Pennsylvania, Philadelphia, Pennsylvania 19104, USA*
[3]*WPI Advanced Institute for Materials Research, Tohoku University, Sendai 980-8577, Japan*
[4]*JST, PRESTO, 4-1-8 Honcho Kawaguchi, Saitama 332-0012, Japan*
(Received 14 March 2012; revised manuscript received 13 April 2012; published 10 May 2012)

We measured the thermal expansion coefficient and Debye temperature of nanoporous gold (NPG) using the extended x-ray absorption fine structure technique. Reduction of the nearest-neighbor distances in NPG by ca. 0.01 Å compared to the bulk gold was attributed to the surface tension caused, in turn, by the finite-size effect of the NPG ligaments. We also demonstrated that the Debye temperature in NPG is 5% lower than in bulk gold. We interpreted these observations in the framework of a bimodal distribution of surface and bulk bonds with different values of Debye temperature. The surface bonds with low Debye temperature extend within ca. four layers of Au atoms located on the pore surface, in a good agreement with prior resistivity measurements and theoretical predictions.

DOI: 10.1103/PhysRevB.85.195419 PACS number(s): 63.22.Dc, 61.05.cj, 65.40.De

I. INTRODUCTION

Nanoporous gold (NPG) received much attention during the last decade as an unsupported catalytic system[1–3] and as an attractive material in the field of sensors,[4] actuators, and optics.[5] Its enhanced catalytic properties for CO oxidation are often attributed, much like in nanoparticle catalysts, to the presence of undercoordinated Au atoms.[6–8] Among other factors that have been recently discussed in terms of their potential influence on the catalytic activity of NPG are surface-to-volume ratio, mechanical strain, as well as the role of residual Ag.[5]

Among these factors, the strain effect on reactivity in nanoscale metal catalysts is a topic of intense experimental and theoretical research. As previously shown, the surface strain-induced change in the metal-metal distances affects adsorbate binding energy.[9,10] Strasser *et al.*[10] interpreted the surface strain effect on reactivity in the framework of the *d*-band center model,[11] by noting that the compressive or tensile strain causes shift in *d*-band relative to the Fermi energy and that, in turn, changes the ligand binding energy. Similar to the static (configurational) disorder of atomic bonds at the surface of nanocatalysts, their nonbulklike dynamic (vibrational) disorder is also predicted to strongly influence their reactivity.[12]

Analogously to metal nanoparticles, structural dynamics of NPG are expected to be modified by the nonbulklike structural and thermal properties of atoms residing in the pore surface. Despite the interest in such finite-size effects in nanomaterials in general, and in the NPG in particular, no reports exist, to the best of our knowledge, on thermal expansion or Debye temperature measurements of the NPG, despite the very intriguing theoretical prediction of its anomalously low value.[13] Such investigations are particularly challenging due to the need to probe both the structure and dynamics of the surface atoms as a function of temperature and pressure and to do so by maintaining high spatial and temporal resolution in order to sense both static and dynamic bond-length characteristics. In this work we applied the extended x-ray absorption fine-structure (EXAFS) method that was successfully used to analyze structural and thermodynamic properties of many bulk[14–16] and nanoscale[17,18] systems. EXAFS is a premier technique for investigations of nanomaterials due to its excellent spatial resolution (the bond lengths can be obtained with an accuracy of 0.005 Å or better) and its sensitivity to atomic vibrations, including anharmonic contributions.[19,20]

In the next section, we present experimental details on synthesis, scanning electron microscopy (SEM) characterization, and EXAFS measurements of NPG. Sec. III describes the data processing and analysis. Results are presented in Sec. IV, and their discussion is given in Sec. V. Conclusions are presented in Sec. VI.

II. EXPERIMENTAL DETAILS

NPG is prepared by dealloying of Au alloy with other component, most commonly, Ag.[21,22] The precursor $Ag_{65}Au_{35}$ (atomic ratio) leaves with dimensions of 20 mm × 20 mm × 700 nm were annealed at 573 K for 3 h to eliminate strain effect. Free-standing NPG sheets were then fabricated by chemically dealloying precursor thin films in a 69% HNO_3 solution for 1 h at room temperature. The dealloyed samples were rinsed by deionized water (18.2 MΩ·cm) for more than three times to remove the residual chemical substances within the nanopore channels.

The morphology and structure of the NPG were investigated using a field-emission scanning electron microscope (JEOL JIB-4600F, 15 keV). A cyclic voltammograms of NPG membrane in 0.1 M $HClO_4$ solutions was obtained with an electrochemical workstation (Ivium Technology). The surface area was estimated using the reduction peak of the Au oxide. The characteristic ligament length scale was measured using fast Fourier transform (FFT) method.[23]

EXAFS data were acquired at beamlines X19A and X18B of the *National Synchrotron Light Source* (NSLS) at Brookhaven National Laboratory in transmission mode using the Au L_3 edge. The samples were prepared by stacking several NPG foils to provide sufficient absorbance (that corresponded to the edge jump of ca. 0.6) at the Au L_3 edge. The sample was

loaded into the dedicated cell for EXAFS studies[24] that can be carried out within a temperature range from ca. 130 K to ca. 800 K. A bulk Au foil was measured simultaneously with the NPG sample (in reference mode) for energy alignment and calibration purposes. Multiple scans (up to four) were collected at each temperature of interest and averaged in order to improve the signal-to-noise ratio. Measurements were done at different temperatures under H_2 (5% H_2 balanced with He for a total flow rate of 50 ml/min) atmospheres. Bulk Au and Ag samples were also measured in the same conditions and similar temperatures as the NPG samples. The lowest temperatures were 133 K (bulk Au), 163 K (NPG), and 183 K (bulk Ag). The rest of the temperatures were the same for all samples studied: 298, 393, 488, 583, and 673 K. As the structure of NPG is reported to coarsen when annealed at temperatures above 423–473 K,[4] the last two temperature points were used for evaluating coarsening effects on EXAFS data.

III. DATA PROCESSING AND ANALYSIS

In EXAFS technique, the information about structural environment, including its dynamic changes, of the x-ray absorbing atom and its surroundings is extracted from the x-ray absorption coefficient $\mu(E)$ measured within 1000–1500 eV from the x-ray absorption edge energy. The oscillatory part of $\mu(E)$ results from the interference patterns of photoelectrons due to their scattering from neighboring atoms. It, thus, contains quantitative information about the local atomic environment in the proximity of the absorbing atom. The EXAFS signal $\chi(k)$ that originates from the nearest group of neighbors at approximately equal distances from the absorbing atoms (i.e., within the first shell) is often written as[25]

$$\chi(k) = \frac{S_0^2 N}{kR^2} |f^{\text{eff}}(k)| \sin\left[2kR - \frac{4}{3}\sigma^{(3)}k^3 + \delta(k)\right] \times e^{-2\sigma^2 k^3} e^{-2R/\lambda(k)}, \quad (1)$$

where k is the photoelectron wave number, $f^{\text{eff}}(k)$ and $\delta(k)$ are the photoelectron scattering-path amplitude and phase, respectively, S_0^2 is the passive electron reduction factor, N is the degenacy of the scattering path (equal to the coordination number for the single-scattering paths), R is the effective half-path length (which equals the interatomic distance for single-scattering paths), σ^2 is the mean-square deviation in R, also known as the second cumulant of the pair distribution function,[26] $\sigma^{(3)}$ is the third cumulant, and $\lambda(k)$ is the photoelectron mean-free path.

In order to extract thermal and structural parameters of NPG from EXAFS data, we applied the correlated Einstein model[27] that proved effective in many previous studies of bulk[28,29] and nanoscale[30–33] metals. In this model, parameters k_0 and k_3 of the anharmonic potential, $V(x) = (1/2)k_0x^2 + k_3x^3$, where $x = r - r_0$ is the deviation of the bond length r from the location of the potential minimum, can be obtained from the temperature dependence of the second and third cumulants of the effective pair distribution function.[27] The same two cumulants can be used to approximate the thermal expansion coefficient, α. In the limit of high temperature (where the quantum effects are negligible), Frenkel and Rehr obtained[27]

$$\sigma_d^2 \cong \frac{k_B T}{k}; \quad \sigma^{(3)} \cong -\frac{6k_3}{k^3}(k_B T)^2; \quad \alpha \cong -\frac{3k_3 k_B}{k^2 r}, \quad (2)$$

where σ_d^2 is the mean-square vibrational (dynamic) bond-length disorder, T the absolute temperature, $k = k_0 + 6k_3\langle y\rangle$ the effective spring constant, y is the deviation from the equilibrium value of x at temperature T, and the brackets denote a thermal average.

Data processing and analysis were performed with the IFEFFIT package.[34] The useful data ranges in k-space varied from 2 to 18.5 Å^{-1} at the lowest temperatures to 2–10.5 Å^{-1} at the highest temperatures. Data fitting was performed by calculating theoretically the photoelectron scattering functions for the first shell Au-Au contribution in bulk Au using the FEFF6 program.[25] They were combined into the EXAFS Eq. (1), which contains electronic (S_0^2, and the photoelectron energy origin correction, ΔE_0) and structural parameters (e.g., N, R, σ^2, and $\sigma^{(3)}$). These parameters were adjusted for all temperature data concurrently by applying multiple constraints in the analysis. The disorder parameters at all temperatures were constrained to follow the correlated Einstein model,[27] which allowed separate evaluation of the temperature-independent, static disorder and the temperature-dependent, dynamic disorder:[30] $\sigma^2(T) = \sigma_s^2 + \sigma_d^2(T)$. The last term on the right-hand side is simply related to the Einstein temperature Θ_E via the effective spring constant in Eq. (2), $k = \mu\omega^2$, where μ is the reduced mass of the atomic pair and $\omega = k_B\Theta_E/\hbar$ is the effective bond vibration frequency (the mean of the projected density of modes).[27] Using the approximate relationship[35] $\Theta_D \approx 1.27\Theta_E$ between the Debye and Einstein temperatures, we also estimated Debye temperatures of Au, Ag, and NPG after the best fit values of Einstein temperatures were obtained.

In the fits to the bulk metals (Au and Ag), the coordination numbers of the first nearest-neighbor (1NN) bonds were fixed at 12 as expected in the face-centered-cubic lattice. The best fit values of S_0^2 were found to be 0.873(14) and 0.947(19), respectively. In order to break the correlation between the amplitude factors in the fit, the S_0^2 parameter of the NPG was fixed to that of bulk Au (0.873). The following parameters were varied in the EXAFS analysis: the corrections to the photoelectron energy origin (the same at all temperatures), the Au-Au coordination number (the same at all temperatures), the nearest-neighbor bond lengths (six variables), the third cumulant of the 1NN pair distribution function (six variables), and the values of Θ_E and σ_s^2. The total number of relevant independent data points was 74, i.e., much greater than the total number of variables (16).

IV. RESULTS

A SEM micrograph of the as-prepared NPG is shown in Fig. 1. The average gold ligament size is ca. 21 nm in length, with the minimum ligament width of 5 nm. The surface-to-volume ratio $\eta = A/V$ was measured to be $(9.2 \pm 0.9) \times 10^7$ m^{-1}.

Representative raw EXAFS data in k-space and r-space are shown in Fig. 2. It is evident that the local structure in NPG is different from that in Au foil, and the difference is

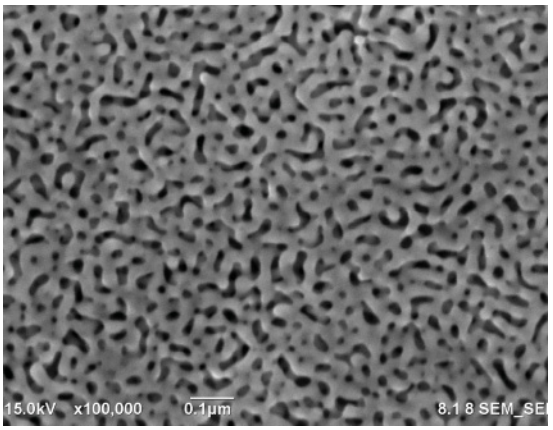

FIG. 1. SEM micrograph of NPG foil with characteristic ligament length scale of ca. 21 nm in length.

particularly noticeable in the 1NN peak region. The reduction in intensity of the NPG can be caused by either the reduced

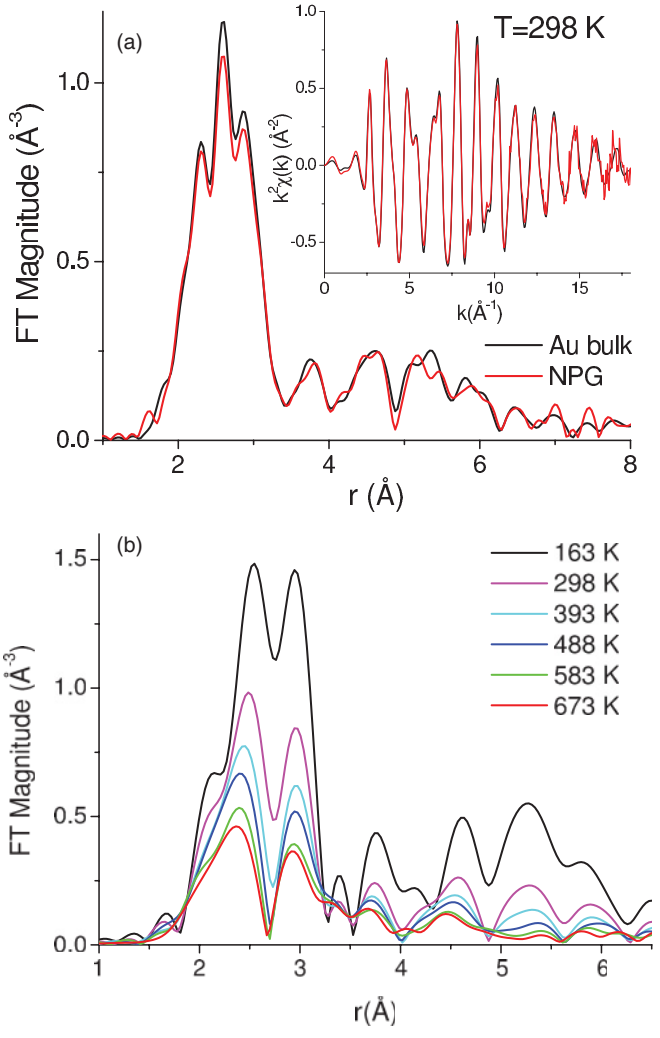

FIG. 2. (Color online) (a) k^2-weighted (inset) and Fourier transform magnitudes EXAFS data for the Au bulk and the NPG samples measured at 298 K. The k range in Fourier transforms was from 2 to 18 Å^{-1}. (b) Fourier transform magnitudes of the k^2-weighted EXAFS data of the NPG measured at different temperatures. The k range for Fourier transforms was from 2 to 12 Å^{-1}.

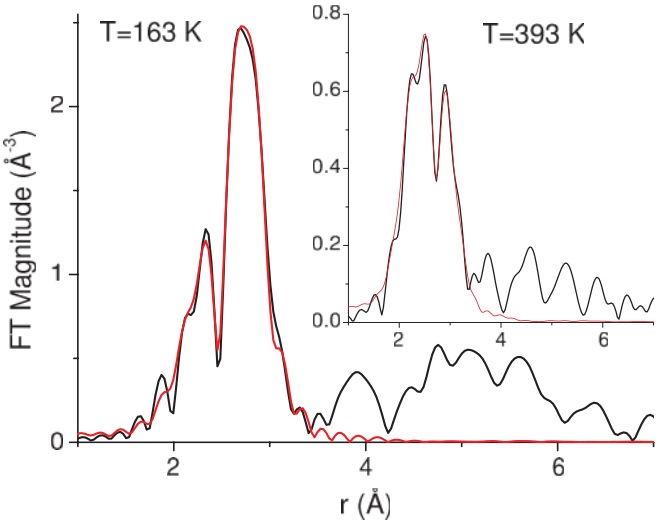

FIG. 3. (Color online) Fourier transform magnitudes of the k^2-weighted data (black) and fit [red (medium gray)] of the NPG samples measured at the 163 and 393 K (inset) temperatures. The k ranges for Fourier transforms were from 2.4 to 18.5 Å^{-1} and from 2.4 to 15.0 Å^{-1}, respectively. The fitting ranges were from 2.0 to 3.4 Å and from 1.7 to 3.4 Å, respectively.

coordination number compared to the bulk, the increased bond-length disorder, or both. Although it is possible to separately evaluate these two effects in nanoparticles, where the coordination numbers are much smaller than in their bulk counterparts,[36–38] in the case of the NPG, the discrimination between these two contributions at the single temperature is complicated. Obtaining this information from EXAFS is much easier by using the strong temperature dependence of EXAFS amplitude and phase [Fig. 2(b)]. In the case of the NPG, where the coordination number of the Au-Au pairs is expected to be close to 12 (and it was obtained to be nearly 12.0, within the ± 0.3 experimental uncertainty), we fixed the coordination number to be the same at all temperatures and separately obtained the best fit results for the coordination number and the values of $\sigma^2(T)$. Additional details are evident in Fig. 2(b). As the temperature increases, the mean 1NN peak position shifts to lower r values. It would have been unphysical for bulk metals with close-packed structure to show negative thermal expansion (NTE),[39] but in this case the explanation is not the NTE but the anharmonicity of the Au-Au pair potential. Indeed, as was obtained before for bulk Pt, the anharmonic correction to the pair potential increases with temperature, and, hence, the phase of EXAFS oscillation may decrease (and thus the peaks shift to the left) despite the increase in the 1NN bond length with temperature.[30] Representative data and fits are shown in Fig. 3 for two different temperatures. The best fit results for the Au-Au distances are shown in Fig. 4. The second and the third cumulants of the pair distribution function are shown in Figs. 5(a) and 5(b), respectively, together with the linear fits with Eq. (2). Table I contains the best fit values of the Einstein and Debye temperatures of bulk Au, Ag, and the NPG, as well as their thermal expansion coefficients, effective force constants k, and the anharmonic parameter k_3 obtained from the fits of Eq. (3) to the experimental data on the second and third cumulants.

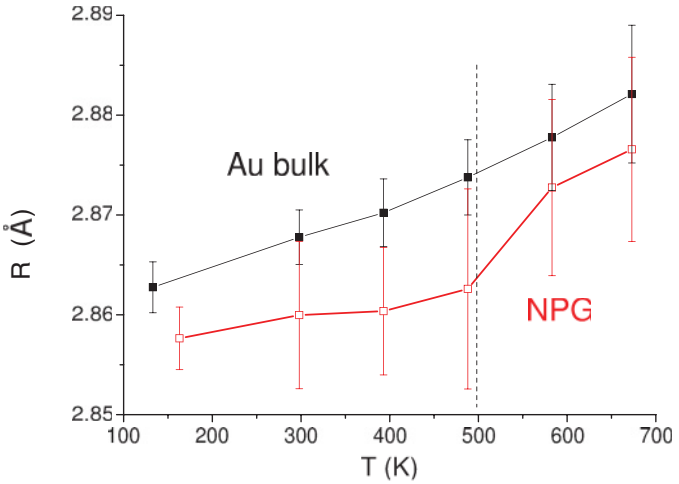

FIG. 4. (Color online) Au-Au distances in the bulk Au and NPG. Connecting lines are guides to the eye. Vertical line indicates the temperature (500 K) above which NPG coarsens.

V. DISCUSSION

The Au-Au distances in the NPG decrease significantly compared to the bulk Au at temperatures less than 500 K, i.e., below the temperature when the NPG starts coarsening (Fig. 4). Such reduction cannot be explained by residual Ag present in our NPG sample after dealloying. Indeed, Au-Ag alloy shows very little change in Au-Au distance with concentration of Ag.[40] In the NPG, we estimated (by relative Au and Ag edge step analysis) the concentration of residual amount of Ag as 6%. Ag K-edge EXAFS data indicate that it is predominantly alloyed with Au. For such a small concentration of Ag, temperature dependence of Au-Au bond of the bulk Au-Ag alloy was shown to be virtually the same as in bulk Au,[40] contrary to what we observed in the NPG (Fig. 4). Therefore, we conclude that the large reduction in Au-Au distance in the NPG compared to the bulk is likely the result of finite-size effects rather than alloying with Ag. Kluth *et al.* reported that the 0.01-Å bond-length contraction (relative to the bulk) in Au nanocrystals as large as 8.5 nm in size,[41] i.e., comparable to the size of ligaments of our NPG, where the minimum width obtained was 5 nm. Our results suggest that the bond-length contraction in NPG has the same origin (surface tension) as in other low-dimensional, unsupported Au systems.[42]

Debye temperatures for bulk Au and Ag obtained in our analysis (Table I) are in good agreement with other measurements (e.g., 175 K[43] and 184.6 K[44] for Au and 225 K[43] for Ag). Thermal expansion coefficients obtained for bulk Au and Ag (Table I) agree well with their reported values: $1.4(1)\times10^{-5}$ K^{-1}[45] and 1.5×10^{-5} K^{-1},[46] respectively. We conclude by noting a good agreement between our EXAFS results and those from literature for thermodynamic properties of bulk Au and Ag and that our procedure is well calibrated on standard compounds and can be applied to investigate the unknown, i.e., the NPG. The intriguing new results obtained for the NPG are the reduction of the Einstein and, hence, Debye temperatures (Table I).

The nanoscale size effect on Debye temperature is far from being understood. Although it is well established that the surface atoms and inner atoms have different vibration

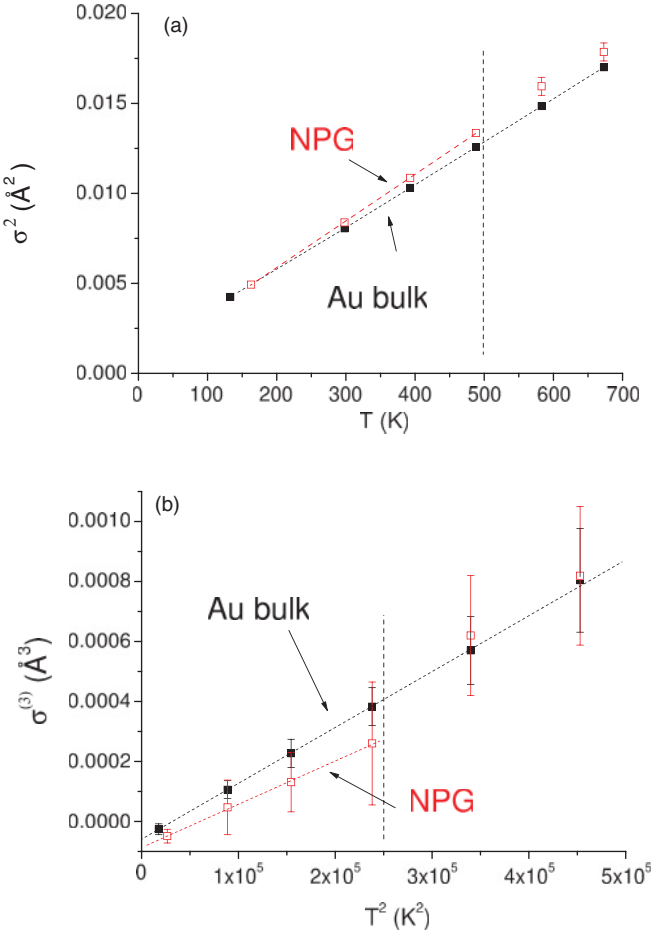

FIG. 5. (Color online) (a) Mean square Au-Au bond-length disorders in the bulk Au and NPG. Best fits with Eq. (1) to each series are shown as dashed lines. The increase in slope in the NPG data relative to the bulk indicates the decreased force constant (and thus decreased Einstein and Debye temperatures) in the NPG compared to the bulk. (b) The third cumulants of the Au-Au bond in the bulk Au and NPG shown as a function of T^2. Best fits with Eq. (2) are shown as dashed lines. Vertical lines correspond to the temperature (500 K) above which NPG coarsens.

frequencies (and thus the surface layer and the interior of the crystal should have different Debye temperatures),[47] the magnitude, and even the sign, of the effect depend very strongly on a particular system. For example, reduction of Debye temperature to 160 K has been previously observed in the smallest Au nanoparticles supported on amorphous silica in the 2.4- to 5-nm range and attributed to the finite-size effect causing the surface atoms to have a smaller vibrational frequency compared to the bulk.[48] In Pt nanoparticles supported on γ-alumina, the opposite effect was observed: their Debye temperature was greater than in the bulk Pt.[31,32] This effect was attributed to the substrate-induced strain.[32] Generally, the finite-size effects are predicted to cause significant deviations of Debye temperature from its bulk limit for very small particle sizes: for Au, the nanoparticle size should be smaller than 5 nm, for its Debye temperature to start decreasing relative to the bulk.[47]

Experimental data that can be used to obtain Debye temperature in NPG are scarce, and so are theoretical estimations.

TABLE I. Numerical results for the Einstein and Debye temperatures, linear thermal expansion coefficient, and pair potential parameters obtained by EXAFS analysis in bulk Au, Ag, and NPG.

	Θ_E (K)	Θ_D (K)	α (K^{-1}) ($\times 10^5$)	k (N/m)	k_3(N/m^2) ($\times 10^{-11}$)
Au bulk	143(1)	182(2)	1.4(1)	58.5(2)	− 3.3(3)
Ag bulk	178(2)	226(3)	1.5(2)	49.3(2)	− 2.5(3)
NPG	137(2)	174(2)	1.0(4)	53.1(1)	− 1.9(7)

Fujita *et al.*[49] report very similar phonon scattering in NPG to bulk gold, indicating a similarity in phonon density of states and thus similar Debye temperatures for NPG and bulk gold. Our result for $\Theta_D = 174$ K in NPG (Table I) is in agreement with that work. On the other hand, this high value Θ_D is in contrast with the theoretical predictions of Xia *et al.*[13] of very low Debye temperature (23 K) in NPG. In that work, Debye temperature was estimated from the bulk elastic constants.

One important conclusion from the combination of all thermodynamic data collected in this experiment is that the metallic bonding in the NPG is anisotropic. Had it been isotropic, the ensemble-average pair distribution function would have been unimodal, and the average Au-Au pair would be characterized by an effective pair potential with the force constant k, *vide supra*. As shown in Table I, the force constant in the NPG is smaller than in bulk Au. Hence, the Au-Au bonds in NPG should be shifted from their equilibrium positions corresponding to $\langle y \rangle = 0$ at any given temperature, namely, their lengths should increase relative to the bulk, because $k = k_0 + 6k_3\langle y \rangle$ and k_3 is negative [Eq. (2) and Table I]. In our experiment, we observe a marked decrease, not an increase, of the average bond length in the NPG relative to the bulk, i.e., the experimentally determined $\langle y \rangle$ was negative, not positive (Fig. 4), which contradicts the assumption that the bond-length distribution is unimodal.

We find that our system can be better described using the model of Kästle *et al.*,[44] who proposed that the phonon spectrum of gold thin films is a superposition of the bulk and the surface spectra, weighted with the surface-to-volume fraction of Au atoms. In that work, Kästle *et al.* followed theoretical calculations of Al Rawi *et al.* to assume that three layers of Au atoms have the same low Debye temperature.[50] They further proposed that the rest of the atoms have the bulklike Debye temperature, $\Theta_{D,bulk}$.[44] The surface value $\Theta_{D,surface} = 83$ K was found from low energy electron diffraction (LEED) experiments on (111) and (110) surfaces, and 82 K was obtained for (100) surface in Au single crystals.[51] We adopt a similar approach by assuming that the bond-length disorder of the 1NN Au atoms is enhanced when the both atoms are near the pore surface, while the disorder is bulklike for the rest of the bonds. Because each group of bonds must have unique Debye temperatures, we can therefore approximate the apparent Debye temperature $\tilde{\Theta}_D$ as the weighted average of the bulk and surface Debye temperatures

$$\tilde{\Theta}_D = \frac{N_B}{N}\Theta_{D,bulk} + \frac{N_S}{N}\Theta_{D,surface}, \quad (3)$$

where N_B and N_S are the corresponding numbers of 1NN Au-Au bonds, and N is the total number of the 1NN bonds. The numbers of each type of bond can be expressed in terms of the total numbers of atoms within each group (bulk, n_B, or surface, n_S) and their respective coordination numbers of nearest neighbors $Z_B = 2N_B/n_B, Z_S = 2N_S/n_S$, yielding

$$\tilde{\Theta}_D = \frac{Z_B}{Z_B + Z_S\xi}\Theta_{D,bulk} + \frac{Z_S\xi}{Z_B + Z_S\xi}\Theta_{D,surface}, \quad (4)$$

where ξ is the surface-to-volume ratio of Au atoms. We assume that the surface Au atoms with the lower Debye temperature are located within m monolayers from the (111)-terminated pore surface (this choice ensures that the so obtained value of m is the upper limit of the number of surface layers). The volume occupied by these surface atoms is $V_0 = mdA$, where $d = 2.35$ Å is the d_{111} spacing for Au, and A is the total surface area of the NPG pores. Within this approximation, ξ can be evaluated as

$$\xi = \frac{n_S}{n_B} = \frac{V_0/V}{1 - V_0/V} = \frac{md\eta}{1 - md\eta}, \quad (5)$$

where $\eta = A/V = 9.2 \times 10^7 m^{-1}$, as described in Sec. IV. Using the measured values of $\tilde{\Theta}_D = 174$ K, $\Theta_{D,bulk} = 182$ K (Table I), and $\Theta_{D,surface} = 83$ K (Ref. 51) and assuming that $Z_B = Z_S = 12$ (as expected for face-centered-cubic structure), we use Eqs. (4) and (5) to estimate m, the number of surface layers with the lower Debye temperature. We obtain the upper limit of $m = 3.7 \pm 0.4$, in good agreement with Kästle *et al.*[44] (*vide supra*) and Al-Rawi *et al.*,[50] who estimated theoretically that enhancement of atomic disorder near the surface may affect atoms as deep as three layers from the surface. The experimental uncertainty in m is dominated by uncertainty in η, which has a relative error of 10%.

VI. CONCLUSIONS

In conclusion, our measurements of structural and vibrational characteristics of NPG resulted in several new effects that are markedly nonbulklike. We demonstrated that the Au-Au interatomic distances, the thermal expansion coefficient, and the Debye temperature are all reduced compared to the bulk gold. Reduction of the nearest-neighbor distances in NPG by ca. 0.01 Å compared to the bulk is attributed to the surface tension caused, in turn, by the finite-size effect of the NPG ligaments. Reduction of the Debye temperature in NPG by 5% compared to bulk gold was interpreted in the framework of the bimodal distribution of surface and bulk bonds. Using this model and the previously measured value of surface Debye temperature, we estimate that the surface bonds with low Debye temperature extend within four layers of Au atoms located on the pore surface.

These findings indicate that the properties of NPG are affected by the dimensions of the NPG ligaments that influence both the Au-Au distance reduction, and the surface-to-volume ratio of Au atoms responsible for the Debye temperature reduction. Because both the pore size and the size of the ligaments can be controlled by the NPG dealloying time,[52] our results offer a possibility to rationally design the NPG with the desired thermodynamic properties. An additional opportunity that emerges from measuring the set of pair potential characteristics in the NPG is the possibility to control the static and dynamic bond-length disorder via the amount of strain in the films by varying their annealing time. Nanoscale strain is an important descriptor of catalytic activity of nanocatalysts, and our analysis method offers a direct method of its control and evaluation. Further studies are required to confirm such capabilities, and they are presently underway.

ACKNOWLEDGMENTS

A.I.F. and R.V. acknowledge the support of this work by the US Department of Energy (DOE) Grant No. DE-FG02-03ER15476. X19A and X18B beamlines are supported, in part, by the Synchrotron Catalysis Consortium (US DOE Grant No. DE-FG02-05ER15688). B.D. and D.L. were supported as part of the Catalysis Center for Energy Innovation, an Energy Frontier Research Center funded by the US DOE, Office of Science, Office of Basic Energy Sciences under Award Number DE-SC00010004. This research was partly supported by JST-PRESTO and the Sekisui Research Foundation.

*frenkel@bnl.gov

[1] A. Wittstock, V. Zielasek, J. Biener, C. M. Friend, and M. Bäumer, Science **327**, 319 (2010).
[2] V. Zielasek, B. Jürgens, C. Schulz, J. Biener, M. M. Biener, A. V. Hamza, and M. Bäumer, Angew. Chem. Int. Ed. Engl. **45**, 8241 (2006).
[3] C. Xu, J. Su, X. Xu, P. Liu, H. Zhao, F. Tian, and Y. Ding, J. Am. Chem. Soc. **129**, 42 (2006).
[4] S. O. Kucheyev, J. R. Hayes, J. Biener, T. Huser, C. E. Talley, and A. V. Hamza, Appl. Phys. Lett. **89**, 053102 (2006).
[5] A. Wittstock, J. Biener, and M. Bäumer, Phys. Chem. Chem. Phys. **12**, 12919 (2010).
[6] H. Falsig, B. Hvolbæk, I. S. Kristensen, T. Jiang, T. Bligaard, C. H. Christensen, and J. K. Nørskov, Angew. Chem. Int. Ed. Engl. **47**, 4835 (2008).
[7] B. Hvolbæk, T. V. W. Janssens, B. S. Clausen, H. Falsig, C. H. Christensen, and J. K. Nørskov, Nano Today **2**, 14 (2007).
[8] K. P. McKenna and A. L. Shluger, J. Phys. Chem. C **111**, 18848 (2007).
[9] A. Schlapka, M. Lischka, A. Gross, U. Käsberger, and P. Jakob, Phys. Rev. Lett. **91**, 016101 (2003).
[10] P. Strasser, S. Koh, T. Anniyev, J. Greeley, K. More, C. Yu, Z. Liu, S. Kaya, D. Nordlund, H. Ogasawara, M. F. Toney, and A. Nilsson, Nat. Chem. **2**, 454 (2010).
[11] B. Hammer and J. K. Nørskov, Nature **376**, 238 (1995).
[12] K. P. McKenna, P. V. Sushko, and A. L. Shluger, J. Chem. Phys. **126**, 154704 (2007).
[13] R. Xia, J. L. Wang, R. Wang, X. Li, X. Zhang, X.-Q. Feng, and Y. Ding, Nanotechnology **21**, 085703 (2010).
[14] A. Sanson, J. Phys. Condens. Matter **23**, 315401 (2011).
[15] G. Dalba, P. Fornasini, R. Grisenti, and J. Purans, Phys. Rev. Lett. **82**, 4240 (1999).
[16] O. Kamishima, T. Ishii, H. Maeda, and S. Kashino, Solid State Commun. **103**, 141 (1997).
[17] L. L. Araujo, P. Kluth, G. d. M. Azevedo, and M. C. Ridgway, AIP Conf. Proc. **882**, 392 (2007).
[18] M. A. Marcus, L. E. Brus, C. Murray, M. G. Bawendi, A. Prasad, and A. P. Alivisatos, Nanostruct. Mater. **1**, 323 (1992).
[19] E. A. Stern, P. Lĩvŋš, and Z. Zhang, Phys. Rev. B **43**, 8850 (1991).
[20] G. Bunker, Nucl. Instrum. Methods Phys. Res. **207**, 437 (1983).
[21] J. Erlebacher, M. J. Aziz, A. Karma, N. Dimitrov, and K. Sieradzki, Nature **410**, 450 (2001).
[22] Y. Ding and J. Erlebacher, J. Am. Chem. Soc. **125**, 7772 (2003).
[23] T. Fujita and M. W. Chen, Jpn. J. Appl. Phys. **47**, 1161 (2008).
[24] M. S. Nashner, A. I. Frenkel, D. L. Adler, J. R. Shapley, and R. G. Nuzzo, J. Am. Chem. Soc. **119**, 7760 (1997).
[25] S. I. Zabinsky, J. J. Rehr, A. Ankudinov, R. C. Albers, and M. J. Eller, Phys. Rev. B **52**, 2995 (1995).
[26] G. Bunker, Nucl. Instrum. Methods **207**, 437 (1983).
[27] A. I. Frenkel and J. J. Rehr, Phys. Rev. B **48**, 585 (1993).
[28] P. Fornasini, S. a Beccara, G. Dalba, R. Grisenti, A. Sanson, M. Vaccari, and F. Rocca, Phys. Rev. B **70**, 174301 (2004).
[29] K. D. Machado, J. Chem. Phys. **134**, 064503 (2011).
[30] A. I. Frenkel, C. W. Hills, and R. G. Nuzzo, J. Phys. Chem. B **105**, 12689 (2001).
[31] S. I. Sanchez, L. D. Menard, A. Bram, J. H. Kang, M. W. Small, R. G. Nuzzo, and A. I. Frenkel, J. Am. Chem. Soc. **131**, 7040 (2009).
[32] B. Roldan Cuenya, A. I. Frenkel, S. Mostafa, F. Behafarid, J. R. Croy, L. K. Ono, and Q. Wang, Phys. Rev. B **82**, 155450 (2010).
[33] D. J. Sprouster, R. Giulian, L. L. Araujo, P. Kluth, B. Johannessen, N. Kirby, and M. C. Ridgway, J. Appl. Phys. **109**, 113517 (2011).
[34] M. Newville, J. Synchrotron Radiat. **8**, 322 (2001).
[35] P. P. Lottici, Phys. Rev. B **35**, 1236 (1987).
[36] A. I. Frenkel, J. Synchrotron Radiat. **6**, 293 (1999).
[37] A. Frenkel, Z. Kristallogr. **222**, 605 (2007).
[38] A. I. Frenkel, A. Yevick, C. Cooper, and R. Vasic, Annu. Rev. Anal. Chem. **4**, 23 (2011).
[39] G. D. Barrera, J. A. O. Bruno, T. H. K. Barron, and N. L. Allan, J. Phys. Condens. Matter **17**, R217 (2005).
[40] A. I. Frenkel, V. S. Machavariani, A. Rubshtein, Y. Rosenberg, A. Voronel, and E. A. Stern, Phys. Rev. B **62**, 9364 (2000).
[41] P. Kluth, B. Johannessen, V. Giraud, A. Cheung, C. J. Glover, G. de M. Azevedo, G. J. Foran, and M. C. Ridgway, Appl. Phys. Lett. **85**, 3561 (2004).
[42] C. W. Mays, J. S. Vermaak, and D. Kuhlmann-Wilsdorf, Surf. Sci. **12**, 134 (1968).

[43]N. W. Ashcroft and N. D. Mermin, *Solid State Physics* (Holt, Rinehart, Winston, New York, 1976).
[44]G. Kästle, H. G. Boyen, A. Schröder, A. Plettl, and P. Ziemann, Phys. Rev. B **70**, 165414 (2004).
[45]W. B. Pearson, *Handbook of Lattice Spacings and Structure of Metals and Alloys* (Pergamon, Oxford, 1958).
[46]M. Dubiel, S. Brunsch, and L. Troger, J. Synchrotron Radiat. **8**, 539 (2001).
[47]S. Xiong, W. Qi, Y. Cheng, B. Huang, M. Wang, and Y. Li, Phys. Chem. Chem. Phys. **13**, 10648 (2011).
[48]T. Comaschi, A. Balerna, and S. Mobilio, Phys. Rev. B **77**, 075432 (2008).
[49]T. Fujita, H. Okada, K. Koyama, K. Watanabe, S. Maekawa, and M. W. Chen, Phys. Rev. Lett. **101**, 166601 (2008).
[50]A. N. Al-Rawi, A. Kara, and T. S. Rahman, Phys. Rev. B **66**, 165439 (2002).
[51]M. Kostelitz and J. L. Domange, Solid State Commun. **13**, 241 (1973).
[52]L. H. Qian and M. W. Chen, Appl. Phys. Lett. **91**, 083105 (2007).